RSC Advances

PAPER

View Article Online
View Journal | View Issue

Cite this: *RSC Adv.*, 2023, **13**, 26640

Investigating the impact of inbuilt cold atmospheric pressure plasma on molecular assemblies of tryptophan enantiomers: *in vitro* fabrication of self-assembled supramolecular structures†

Deepjyoti Basumatary,[ab] Heremba Bailung,[a] Sachin B. Jorvekar,[c] Roshan M. Borkar[c] and Kamatchi Sankaranarayanan *[a]

The advancements in understanding the phenomenon of plasma interactions with matter, coupled with the development of CAPP devices, have resulted in an interdisciplinary research topic of significant importance. This has led to the integration of various fields of science, including plasma physics, chemistry, biomedical sciences, and engineering. The reactive oxygen species and reactive nitrogen species generated from cold atmospheric plasma on interaction with biomolecules like proteins and peptides form various supramolecular structures. CAPP treatment of amino acids, which are the fundamental building blocks of proteins, holds potential in creating self-assembled supramolecular architectures. In this work, we demonstrate the process of self-assembly of aromatic amino acid tryptophan (Trp) enantiomers (L-tryptophan and D-tryptophan) into ordered supramolecular assemblies induced by the reactive species generated by a cold atmospheric pressure helium plasma jet. These enantiomers of tryptophan form organized structures as evidenced by FE-SEM. To assess the impact of CAPP treatment on the observed assemblies, we employed various analytical techniques such as zeta potential, dynamic light scattering and FTIR spectroscopy. Also, photoluminescence and time-resolved lifetime measurements revealed the transfiguration of individual Trp enantiomers. The LC-ESI-QTOF-MS analysis demonstrated that CAPP irradiation led to the incorporation of oxygenated ions into the pure Trp molecule. These studies of the self-assembly of Trp due to ROS and RNS interactions will help us to understand the assembly environment. This knowledge may be utilized to artificially design and synthesize highly ordered functional supramolecular structures using CAPP.

Received 17th June 2023
Accepted 28th August 2023

DOI: 10.1039/d3ra04086k

rsc.li/rsc-advances

1. Introduction

Amino acids play a crucial role in the synthesis of peptides and proteins, such as antibodies and cytokines, and they also regulate important metabolic pathways that are essential for the health and survival of the human body.[1–4] In nature, amino acids self-assemble themselves into functional peptides and proteins through the molecular self-assembly process.[5] Aromatic amino acids such as phenylalanine, tryptophan, tyrosine, and histidine depending on the physiological and chemical conditions that they are subjected to, have been reported to form various supramolecular self-assembled nanostructures like fibres, nanotubes, nanoribbons, twisted nanosheets, dendritic structures, *etc.*[6] Also, these aromatic amino acids are crucial hot spots for the acceleration of several neurodegenerative diseases and amyloidosis.[7] Overproduction of ROS and RNS due to oxidative stress has been identified as one of the biological parameters that trigger abnormalities of amino acids, thereby causing chronic diseases.[8] To understand the molecular assembly mechanism of amino acids, *in vitro* assessments are required. An emerging technique, called CAPP showed physical as well as chemical modifications of these amino acids in aqueous solutions due to ROS and RNS,[9] and could lead to the formation of supramolecular self-assembled architectures which could be used in therapeutic delivery,[10] disease model study,[11] piezoelectric structure formation,[12] protein folding study,[13] *etc.*

CAPP produces low-temperature plasma fumes in (to) ambient air thereby producing charged species, electric fields, UV radiation, and radicals[14–16] that can be tuned[17] to be non-destructive to biomolecules, cells, tissues and effective in

[a]*Institute of Advanced Study in Science and Technology, (An Autonomous Institute Under DST, Govt. of India), Vigyan Path, Paschim Boragaon, Garchuk, Guwahati 781035, Assam, India. E-mail: kamatchi.sankaran@gmail.com*

[b]*Academy of Scientific and Innovative Research (AcSIR), Ghaziabad 201002, India*

[c]*Department of Pharmaceutical Analysis, National Institute of Pharmaceutical Education and Research (NIPER), Sila Katamur (Halugurisuk), PO: Changsari, Kamrup, Assam 781101, India*

† Electronic supplementary information (ESI) available. See DOI: https://doi.org/10.1039/d3ra04086k

various parasites and microorganism inactivation.[18–21] CAPP generates controllable amounts of ROS and RNS that are transported to react with biological targets including cells and tissues for cancer treatment,[22] sterilization of wound tissue,[23,24] corneal infections treatment,[25] instantaneous blood coagulation,[26] leishmaniosis,[27] treatment of dental diseases[28] and protein modifications.[29,30] Other application areas CAPPs include material etching,[31] depositions,[32] surface modification,[33] degradation of pollutants,[34,35] decontamination of microorganisms in water,[36,37] synthesis of nanomaterials,[38,39] *etc.*, however, its usability in the formation of new materials in aqueous systems still needs more exploration.

In this study, we investigated the self-assembly of the enantiomers of the amino acid Trp, *viz.* L-Trp and D-Trp, under varying treatment times using an inbuilt 4-jet cold atmospheric pressure plasma (4-jet CAPP) jet. We employed microscopy, electrokinetic potential, scattering techniques, and spectroscopy to analyse the self-assembly process. Field emission scanning electron microscopy (FESEM) confirmed the formation of supramolecular structures of Trp enantiomers after plasma irradiation. Additionally, zeta potential and dynamic light scattering measurements were used to determine the magnitude of electrostatic repulsion/attraction between particles and the size distribution of particles. Photoluminescence (PL) and time-resolved fluorescence spectroscopy were performed to investigate emission spectroscopic changes and the effects of π–π stacking interactions as well as the lifetimes of excited states of L-Trp and D-Trp with respect to different treatment times. Fourier transform infrared (FTIR) spectroscopy interpreted molecular changes occurred in tryptophan enantiomers before and after plasma treatment. The MS analysis provided evidence that the CAPP irradiation caused a significant change in the chemical structure of Trp. The results of this study indicate that CAPP irradiation may be a promising approach for altering the self-assembling behaviour of Trp enantiomers, which could have important implications for the development of new supramolecular structures based on simple building blocks. These findings may pave the way for the design of novel nanomaterials with unique physical and chemical properties, which could have a wide range of applications in fields such as medicine, electronics, and energy.

2. Materials and methods

2.1. Materials

All amino acids were purchased from Sigma-Aldrich having 98% purity. The amino acids were dissolved in pH 7.4 phosphate buffer solution of strength 10 mM prepared with type-I resistivity ~18.2 MΩ ultrapure distilled water. All chemicals and reagents were used without further purification.

2.2. Experimental setup

In this experiment, the tryptophan enantiomer solutions were irradiated for different exposure times with an inbuilt 4-jet CAPP, as shown in Fig. 1. The configuration generated higher ROS and RNS dosage in the sample solution with a very little temperature rise of about 1–2 degrees celsius. To obtain a stable glow discharge plasma plume, a 4 kV high voltage of frequency 25 kHz was used to power the device with helium gas maintained with flow rate of 2.5 standard liters per minute. The detailed description of the device used is described in our earlier work.[30]

2.3. Measurement of pH and ROS/RNS generated by CAPP in solution

After plasma irradiation on the sample solutions for 5 and 10 min, pH measurements were carried out and it showed about 0.1 (approx.) pH decrease. The concentrations of hydroxide ion

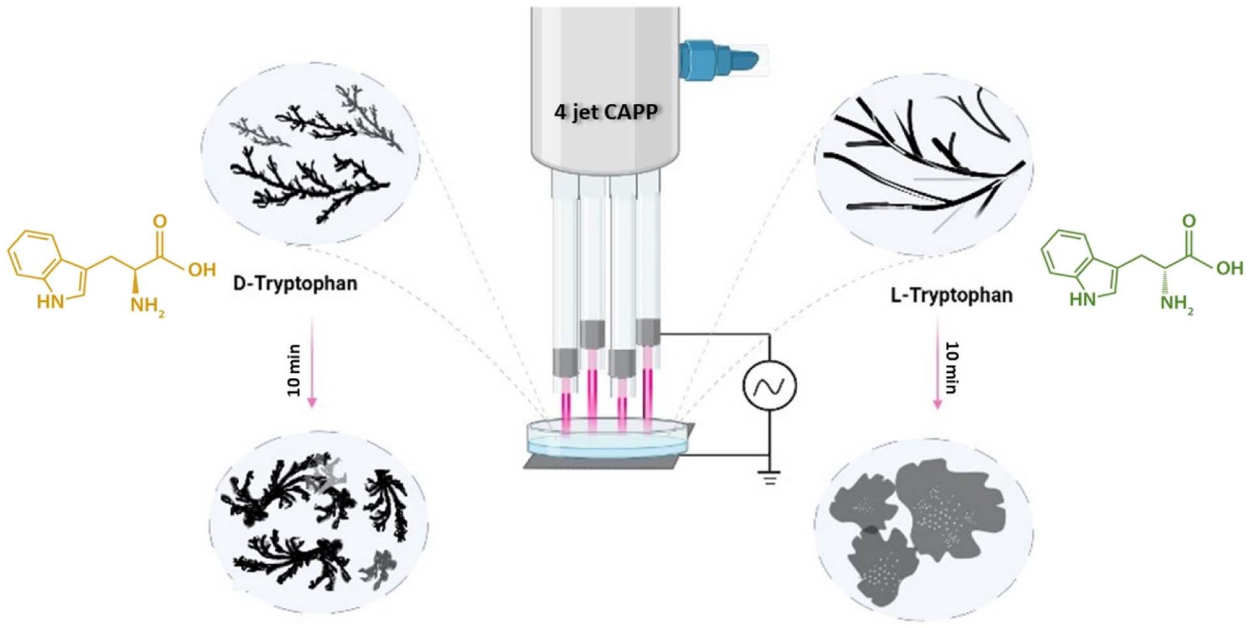

Fig. 1 Schematic representation of 4-jet helium gas CAPP treatment on tryptophan enantiomers causing supramolecular structures.

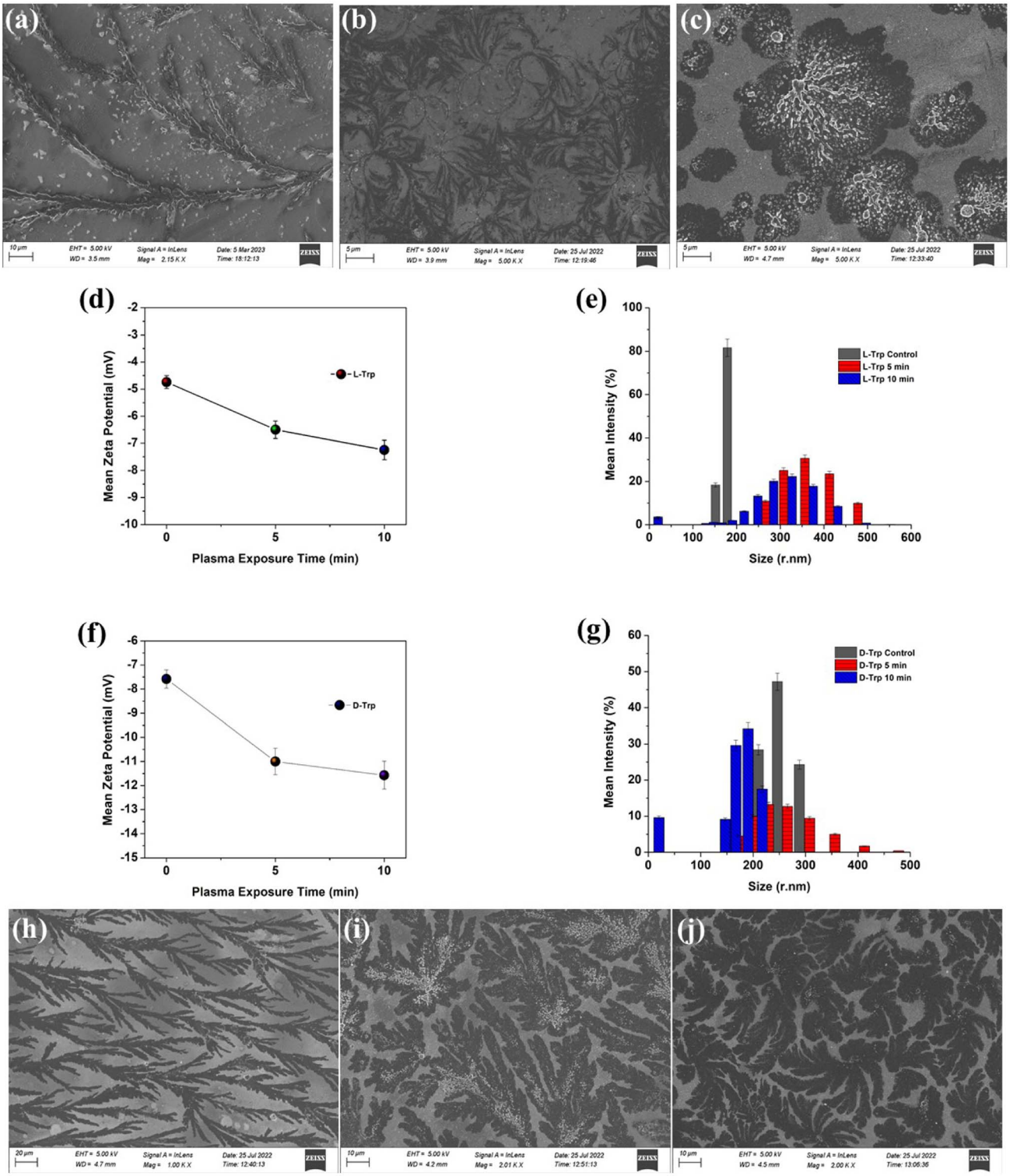

Fig. 2 FE-SEM images of L-Trp (a) control (b) 5 min (c) 10 min and D-Trp (h) control (i) 5 min (j) 10 min of CAP treatment; zeta potential variation of (d) L-Trp (f) D-Trp; DLS size distribution statistical profile of (e) L-Trp (g) D-Trp before and after plasma treatment.

(OH^-) hydrogen peroxide (H_2O_2), nitric oxide (NO), nitrite ion (NO_2^-), and nitrate ion (NO_3^-) were measured in pH 7.4 phosphate buffer solution. The concentration of OH^- was measured by dissolving terephthalic acid (TA) in phosphate buffer solution at 500 μM concentration. Upon plasma exposure, TA reacts with OH^- and creates fluorescent hydroxy terephthalic acid (HTA), and the excitation/emission maxima for the formation of HTA are 312/423 nm. The H_2O_2 concentration was measured using red fluorescence fluorometric hydrogen peroxide assay kit

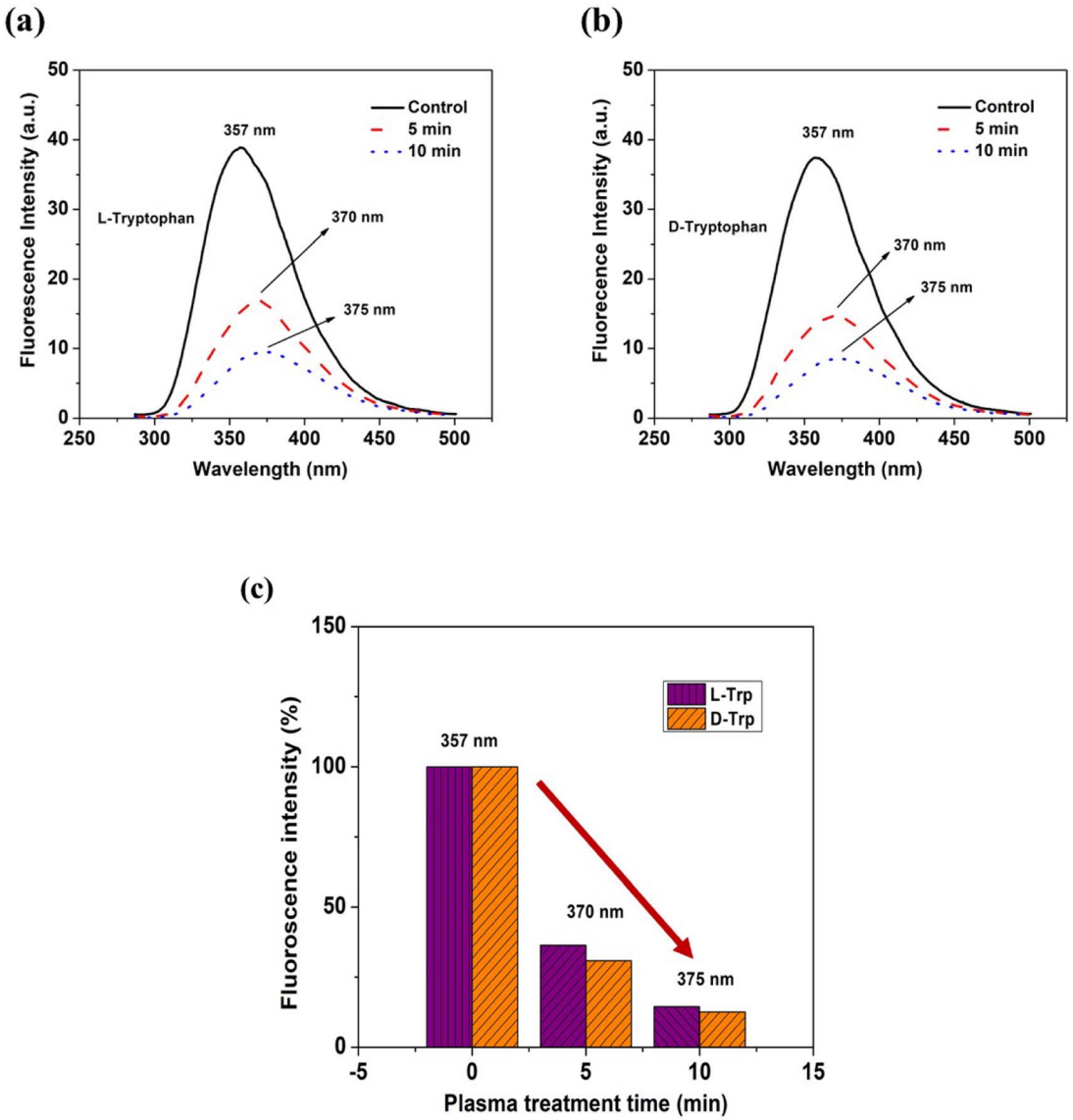

Fig. 3 Fluorescence spectra of (a and b) L-Trp and D-Trp (c) λ_{em} shift and statistical representation of intensity quenching with respect to CAPP treatment time.

by Sigma-Aldrich. NO_2^-, NO_3^- and NO were estimated using Cayman Chemical nitrate/nitrite colorimetric assay kit.

2.4. FE-SEM analysis

Field Emission Scanning Electron Microscopy examined the morphology of the self-assembled supramolecular structures. 10 μL of pure and plasma-treated tryptophan enantiomer solutions were air dried overnight on 1 cm × 1 cm glass slides and then coated with gold–palladium followed by FE-imaging to obtain a top view on a Zeiss SIGMA VP-FESEM electron microscope, operating at 5 kV and a working distance of 3–5 mm.

2.5. Dynamic light scattering and zeta potential

Malvern Analytical Nano ZS90 was used for dynamic light scattering (DLS) and zeta potential measurements of the tryptophan enantiomers.

2.6. Photoluminescence spectroscopy

A concentration of 3 mM concentration of Trp was used for the study. Steady-state fluorescence was measured in a Cary Eclipse Agilent photoluminescence spectrometer of the untreated and plasma-treated tryptophan enantiomer solutions.

2.7. FTIR spectroscopy

PerkinElmer Spectrum 2 FTIR spectrophotometer was used for recording 4000–400 cm^{-1} IR spectra of untreated and plasma-treated lyophilized tryptophan samples using a diamond crystal in total reflection mode.

2.8. Time-resolved photoluminescence spectroscopy

Emission lifetimes were measured on LifeSpec II, Edinburg picosecond time-resolved photoluminescence spectrophotometer

(QM08075-21-C, Horiba) with a 295 nm LED excitation source. The lifetime of the samples was calculated by fitting the decay profiles in F980 software.

2.9. Liquid chromatography quadrupole time-of-flight mass spectrometry (LC-ESI-QTOF-MS) analysis and sample preparation

Identification of Trp and modified Trp compounds was carried out using LC-ESI-QTOF-MS, which was coupled with an Agilent 1290 Infinity II HPLC system equipped with dual Agilent jet stream electrospray ionization. Chromatographic separation was achieved using a ZORBAX Eclipse C18 column, and a mobile phase gradient consisting of 0.1% formic acid in MilliQ water (A) and 0.1% formic acid in methanol (B). The mass spectrometer was operated in positive ESI mode with optimized source conditions, and full scan data were acquired over a mass range of 50–750 *m*/*z*. Sample preparation involved dissolving 1 mg of the sample in 1 mL of methanol, followed by vortexing, filtering through a syringe filter, and injecting 10 μL of the filtered solution into the mass spectrometry system for analysis. The flow rate was 0.4 mL min^{-1}, the column temperature was maintained at 45 °C, and the injection volume was 10 μL.

2.10. XRD study

Study of XRD pattern was performed to evaluate the difference in the arrangement of molecules in untreated and plasma-treated self-assembled tryptophan. About 5 mg of lyophilized samples were characterized by Bruker D8 advanced diffractometer illuminated with source Cu K_α radiation using locked-couple X-ray diffraction technique.

3. Result and discussions

We first dissolved pure L-Trp and D-Trp enantiomers separately in 7.4 pH phosphate buffer solution at concentrations of 3 mM and treated 5 mL of each solution for 5 min and 10 min respectively under 4-jet CAPP maintaining a separation distance of about 2–3 mm between the end of the glass tubes and the Petri dish containing the sample solutions (Fig. 1). The pH values remained unchanged after the treatment, indicating that the treatment did not have a significant impact on the acidity or basicity of the solvent environment.

3.1. CAPP-induced self-assembled supramolecular structures of L-Trp and D-Trp

FE-SEM imaging was used to examine the self-assembly of tryptophan in untreated and plasma-treated sample solutions that were drop-cast onto glass slides. The high-resolution images obtained from FE-SEM allowed for the visualization of the supramolecular structures formed by the tryptophan enantiomers, and the comparison of these structures between the untreated and plasma-treated samples. When L-Trp was subjected to 4-jet helium gas CAPP treatment, the FE-SEM images showed a transformation in the morphology of the self-assembled structures. After 5 minutes of treatment, the leafy-veins-like morphology (Fig. 2(a)) of the L-Trp sample transformed into hair-like follicles (as depicted in Fig. 2(b)). Further treatment for 10 minutes resulted in the formation of larger highly ordered aggregated self-assembled structures (as depicted in Fig. 2(c)). In a similar manner D-Trp molecules also revealed molecular self-assembly transformation. The fibre bundles (Fig. 2(h)) like the morphological structure of pure enantiomer, transformed to digitate finger-like lobes (Fig. 2(i)) after 5 min treatment and highly coordinated clover-like diverse supramolecular structures (Fig. 2(j)) after 10 min treatment. The analysis of the zeta potential (Fig. 2d and f) for both L-Trp and D-Trp showed that the values were negative *i.e.* electrostatic repulsion between identically charged particles in the surroundings. These indicates that the plasma-treated samples are characterized as an anionic colloidal system, where the surface of the particles is negatively charged. The anionic nature of the colloidal system can have significant implications for the stability and behaviour of the supramolecular structures formed by the enantiomers, and may influence their biological

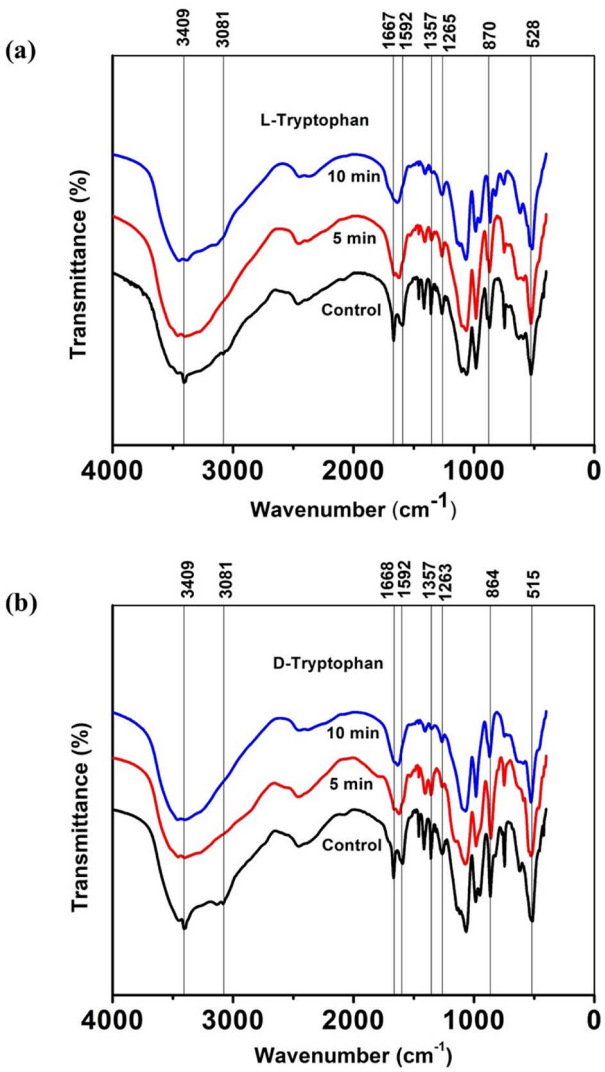

Fig. 4 Variation of FTIR spectra of untreated and CAPP treated lyophilized (a) L-Trp (b) D-Trp.

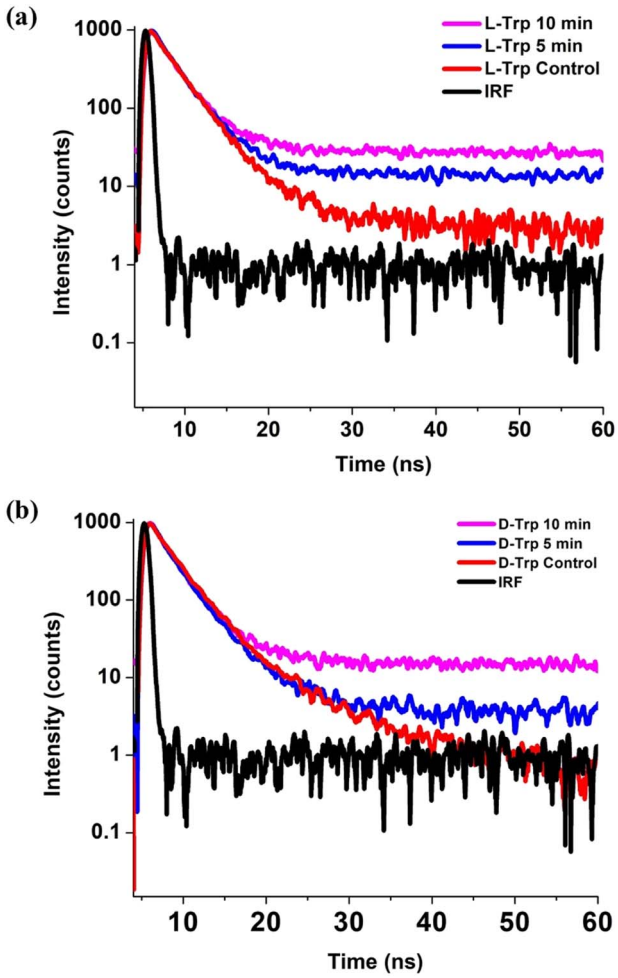

Fig. 5 Time resolved photoluminescence spectra of control, 5 and 10 min He-CAPP treated (a) L-Trp and (b) D-Trp.

and physical properties.[40] Plasma-treated L-Trp and D-Trp samples revealed a significant increase in negative potential. This increased negative potential indicates a shift towards a more stable condition, which can facilitate coagulation and bonding between particles to form larger aggregates. These changes in potential may be attributed to the increase in the polarity of the Trp molecules due to the plasma treatment, which can lead to a higher attraction between particles.[41] To further confirm the changes in the size of the tryptophan molecules, Dynamic Light Scattering (DLS) measurements were carried out. The results of DLS measurements are presented in Fig. 2(e), (g) and Tables S1 and S2,† which show that both L-Trp and D-Trp samples were polydispersed. After 10 minutes of plasma exposure, the mean size of L-Trp increased, indicating the formation of aggregates due to self-assembly. In contrast, the mean particle size of D-Trp decreased, suggesting a different self-assembly process, as observed in the FESEM analysis. The CAPP treatment significantly impacted the formation of self-assembled structures in Trp, resulting in altered properties of supramolecular self-assembled structures with distinct morphologies and sizes of high ordered stability and behaviour. This led to the formation of larger aggregates and potentially resulted in conglomeration.

The steady-state fluorescence studies (Fig. 3(a)–(c)) with λ_{ex} 280 nm revealed intensity quenching and redshift after plasma irradiation possibly due to the increase in polarity of the solvent environment of Trp.[42] Such kind of redshifts in λ_{em} depicts the formation of ordered assemblies arising mainly due to uneven distribution of various concentrations of different molecules. Assemblies like polymer matrixes, glasses, vesicles, micelles, polypeptides, and tissue layers show such arrangements.[43,44] Quenching observed was mainly due to ground-state molecular rearrangements into complex formations which indicate shielding of Trp molecule due to ROS/RNS attached with the molecule after CAPP treatment.[45,46]

3.2. FTIR analysis

To gain a deeper understanding of the molecular interactions responsible for the observed self-assemblies of tryptophan resulting from interactions with CAPP, Fourier Transform Infrared (FTIR) spectra were recorded for lyophilized L-Trp and D-Trp samples in their pure and plasma-triggered self-assembled state. The FTIR spectra are presented in Fig. 4(a) and (b) and were analysed to identify the changes in the molecular structure and functional groups of the tryptophan molecules induced by the plasma treatment. These spectral changes can provide insights into the chemical interactions that drive the self-assembly of the tryptophan molecules. The FTIR analysis is expected to reveal the presence of new functional groups and the disappearance or alteration of existing ones, providing a better understanding of the molecular interactions responsible for the observed self-assemblies. The FTIR spectra analysis revealed several significant changes in the molecular structure and functional groups of the tryptophan molecules induced by the plasma treatment. The intense peak at 3409 cm^{-1} corresponded to indole ring N–H stretching vibration, while the 3081 cm^{-1} vibrations related to aromatic CH merged and became broader.[47,48] These changes were observed more clearly in case of D-Trp than in L-Trp. Similarly, the peak corresponding to C=O stretching at 1668 cm^{-1} of the tryptophan converged with the peak at 1592 cm^{-1} of C=C stretching in the aromatic ring.[49,50] These observations suggest

Table 1 ROS/RNS reactive species generated in the PBS solution on plasma exposure

Treatment time (min)	OH^- (μM)	H_2O_2 (μM)	NO_2^- (μM)	NO_3^- (μM)	NO (μM)
5	14.7 ± 0.9	37.82 ± 1.1	5.39 ± 0.9	4.35 ± 0.4	9.74 ± 0.66
10	12.9 ± 0.24	30.41 ± 0.7	6.27 ± 0.1	5.53 ± 0.3	11.8 ± 0.87

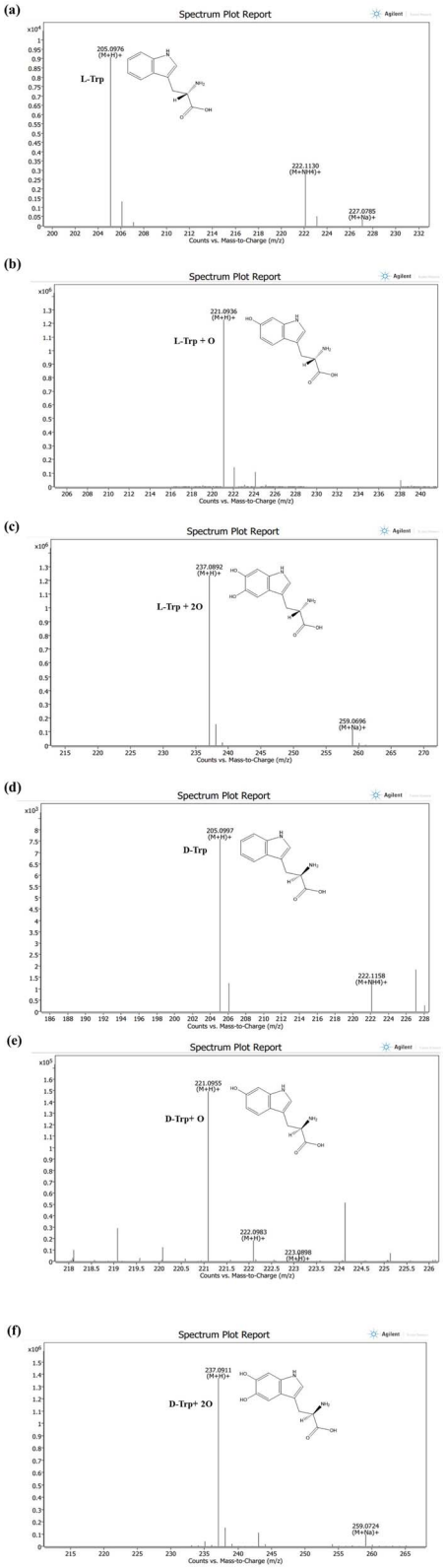

Fig. 6 LC-ESI-MS spectrum of (a) $[M + H]^+$ ions (*m*/*z* 205) of L-tryptophan before plasma treatment (b) $[M + H]^+$ ions (*m*/*z* 221) of mono oxidised L-tryptophan after 5 min plasma treatment (c) $[M + H]^+$ ions (*m*/*z* 237) of di-oxidised L-tryptophan after 10 min plasma treatment (d) $[M + H]^+$ ions (*m*/*z* 205) of D-tryptophan before plasma treatment (e) $[M + H]^+$ ions (*m*/*z* 221) of mono oxidised D-tryptophan after 5 min plasma treatment (f) $[M + H]^+$ ions (*m*/*z* 237) of di-oxidised D-tryptophan after 10 min treatment.

that the plasma-generated ROS/RNS led to the addition of oxygen into the tryptophan molecule, resulting in the amalgamation of most of these vibrations of monomeric tryptophan.

The peak at 1357 cm^{-1} corresponding to the C–N stretching vibration[51] in the indole ring indicated that the self-assembled state of tryptophan exhibited diminished transmittance intensities, implying a relative decrease in the polarities surrounding molecules, mainly due to the well-packed arrangement between molecules after plasma-induced self-assembly. The peaks between 1270 and 1050 cm^{-1} due to stretching vibrations of C–O show similar converging of peaks, while the vibrations under 1000 cm^{-1} representing out-of-plane bending of the aromatics became diminish to some extent after CAPP treatment for both L-Trp and D-Trp.[52] These observations suggest that the plasma treatment induced significant changes in the molecular structure and functional groups of the tryptophan molecules, leading to the observed self-assembled structures.

3.3. Lifetime measurement of the self-assembled enantiomers

To determine the quenching effect, photoluminescence (PL) lifetimes were measured using 295 nm LED excitations for untreated (Fig. 5(a)) and plasma-treated (Fig. 5(b)) tryptophan solutions. The decay lifetimes and constituent components percentage of the emissive states were calculated through the use of time-correlated single photon counting (TCSPC) method, and the multi-exponential decay function was used to fit all decay profiles:

$$F(t) = \Sigma B_i \exp(-t/\tau_i) \quad (1)$$

where B_i and τ_i denote the amplitudes and lifetimes of each component.

The decay profiles of the tryptophan enantiomer solutions were fitted by bi-exponential decay functions (Fig. S1 and S2†), confirming the presence of two emission states of nanosecond (ns) timescale on the tryptophan residue. In L-Trp (Table S3†), we observe the lifetime of control L-Trp sample to be 2.71 ns and 6.71 ns. With the increase in treatment time up to 10 min, the lifetime decreases to 2.25 ns and 4.43 ns, with an increase in % population of τ_2 component and a decrease in τ_1 component (Table S3†), indicating L-Trp undergoing self-assembly as a result decays faster. For D-Trp (Table S4†), the decay time of 2.51 (τ_1) ns and 5.44 (τ_2) ns reduced to 2.08 (τ_1) ns and 3.97 (τ_2) respectively with a similar increase in the % population of τ_2 component and a decrease in τ_1 component (Table S4†), which clearly implies a self-assembly process earlier reported.[53] The higher content of O-element embedment due to plasma treatment in FTIR spectra scan can be correlated to the increase in the contribution of τ_2.

3.4. Measurement of ROS/RNS generated by CAPP

The concentrations of hydroxide ion (OH^-), hydrogen peroxide (H_2O_2), nitrite ion (NO_2^-), nitrate ion (NO_3^-) and nitric oxide (NO) were measured in pH 7.4 phosphate buffer solution.

The concentration of OH^- was measured by dissolving terephthalic acid (TA) in phosphate buffer solution at 500 μM

concentration. Upon plasma exposure, TA react with OH^- and creates fluorescent hydroxy terephthalic acid (HTA), and the excitation/emission maxima for the formation of HTA are 312/423 nm.[21,30] The H_2O_2 concentration was measured using red fluorescence fluorometric hydrogen peroxide assay kit by Sigma-Aldrich. NO, NO_2^- and NO_3^- were estimated using Cayman chemical nitrate/nitrite colorimetric assay kit. Table 1 clearly presents the variation of different radicals and they play a crucial role in the reaction. Trp is readily oxidized by H_2O_2 (ref. 54) and can form different degradation products at different pH. Since the pH did not change in our experiments, the most possible reaction is the oxidation of the Trp. This was further verified with the LC-ESI-QTOF experiment.

3.5. LC-ESI-QTOF analysis of plasma-treated tryptophan

To gain a comprehensive understanding of the impact of ROS/RNS on individual Trp molecules, which led to unusual observations following CAPP treatment in an aqueous solution, an analysis of LC-ESI-QTOF-MS was conducted to explore potential chemical modifications. This analysis aimed to shed light on the mechanisms underlying the observed effects of plasma ROS/RNS on Trp molecules. Fig. 6(a)–(f) shows the LC/ESI/MS total ion chromatogram of Trp CAPP treatment in an aqueous solution. To elucidate the most likely structures of modified Trp, accurate mass measurements were studied. Before plasma treatment, protonated L-Trp and D-Trp were detected with respective molecular ion peaks at m/z 205.0976 and 205.0997 ($[M + H]^+$). The elemental composition of L-Trp and D-Trp was determined as $C_{11}H_{13}N_2O_2$. Both compounds were eluted at 10.3 minutes in the chromatographic analysis. The elemental compositions of protonated ions were confirmed by accurate mass measurements. The LC-ESI-QTOF-MS analysis of CAPP-treated L-Trp molecule in an aqueous solution for 5 min and 10 min shows mono and di-oxidation products at m/z 221.0936 ($[$L-Trp + O + H$]^+$ and 237.0892 ($[$L-Trp + 2O + H$]^+$ with an elemental composition of $C_{11}H_{13}N_2O_3$ and $C_{11}H_{13}N_2O_4$; eluted at 9.4 and 9.2 min, respectively. The increase in 16 Da and 32 Da in products of L-Trp and its elemental compositions indicates mono and di-oxidation products of L-Trp, respectively. Following plasma treatment, the analysis of D-Trp at 5 and 10 minutes revealed the presence of two oxidation products. The first oxidation product exhibited a molecular ion peak at m/z 221.0955, indicating the addition of one oxygen atom. The second oxidation product displayed a molecular ion peak at m/z 237.0911, indicating the addition of two oxygen atoms to the D-Trp molecule. These findings suggest the occurrence of oxidative modifications during plasma treatment.

The plasma treatment led to the oxidation of electron-rich groups in amino acids by various active species. However, there was no observed nitration after plasma treatment, indicating that Trp has low reactivity to RNS. Instead, only hydroxylation of Trp residues was observed (as shown in Fig. S3 and S4†), which is consistent with our previous report that the intrinsic fluorescence of Trp residues in a protein decreases rapidly upon plasma irradiation.[30]

3.6. X-ray diffraction pattern after CAPP treatment

Supramolecular self-assemblies correlate with the tight packing of molecules into organized microstructures. Accordingly, the lattice packing changes between untreated and CAPP-treated tryptophan enantiomers were analyzed using XRD spectra. The diffraction patterns obtained for the treated and untreated self-assembled states in L-Trp were similar, but the untreated state had decreased intensities. After CAPP treatment, intensity of sharp peak at $2\theta = 10.44°$ subsided [Fig. 7(a)]. However, XRD spectra for CAPP treated D-Trp showed new peaks emergence at $2\theta = 19.75°$ and 29.07° with lowered peak intensities like that of L-Trp. Such observations indicate formation of new diffraction plane which differs in packing from untreated D-Trp [Fig. 7(b)]. For both tryptophan enantiomers, disappearance of less intense peaks after CAPP treatment were observed which depicts increasing of ordered bundling of tryptophan molecules in plasma treated self-assembled state.[55] These differences in observed XRD patterns for the untreated and treated forms represents the

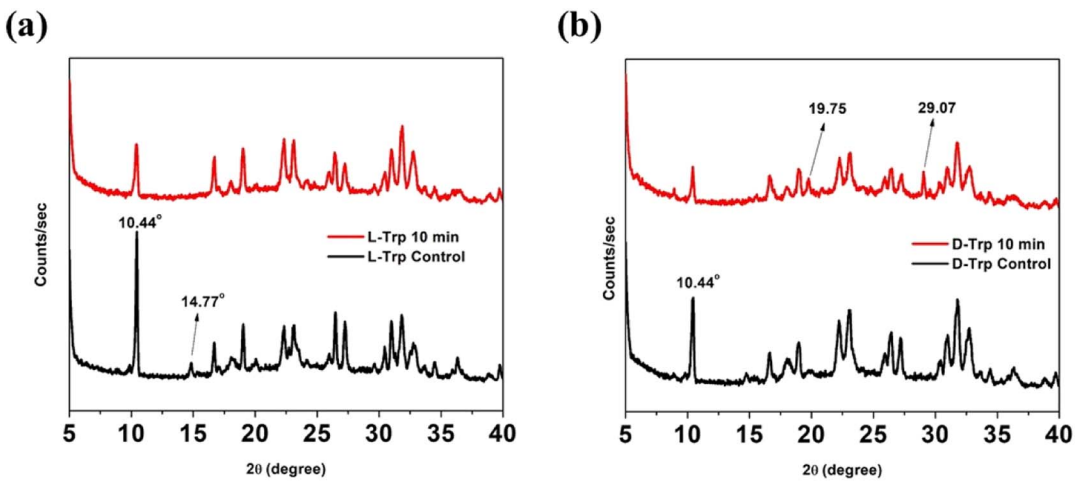

Fig. 7 XRD pattern of control and 10 min CAPP treated (a) L-Trp (b) D-Trp.

difference in packing of molecules which results formation of such self-assembled supramolecular structures of tryptophan enantiomers after CAPP treatment.

4. Conclusion

As a whole, we have assessed the effect of our inbuilt 4-jet helium gas CAPP device on the tryptophan enantiomers. FESEM imaging revealed that upon exposure to ROS/RNS induced by the plasma device in the solvent system, the enantiomers underwent supramolecular self-assembly into distinct architectures. By analysing the mass spectra, it was observed that oxidation of tryptophan occurs through a chemical reaction with the active species generated by CAPP. This finding is crucial for gaining insights into the mechanism of action of active species with biomolecule. Compared to the pure Trp enantiomers, the modified Trp enantiomers have different sizes and are more anionic. The FTIR and TRPL spectra provided additional evidence for the self-assembly process of Trp due to oxygen addition following CAPP treatment, as demonstrated by the increased decay times. The XRD pattern indicated that the plasma-treated Trp molecules had a higher degree of tight packing compared to the untreated Trp molecules, indicating increased stability due to oxidation. The findings of this study indicate that the self-assembly process of Trp enantiomers can be triggered, tuned and controlled by adjusting the ROS/RNS production time during helium gas CAPP treatment. The self-assembly technique demonstrated in this study, utilizing CAPP, has the potential to be further explored for understanding the self-assembly process of many other biomolecules. This, in turn, could lead to the development of novel biomaterials for biomedical engineering applications.

Conflicts of interest

There are no conflicts to declare.

Abbreviations

CAPP	Cold atmospheric pressure plasma
ROS	Reactive oxygen species
RNS	Reactive nitrogen species
LC-ESI-QTOF-MS	Liquid chromatography quadrupole time-of-flight mass spectrometer
PL	Photoluminescence

Acknowledgements

This work was supported by DST-IASST, Guwahati In-house project grant and SRG grant (SRG/2020/001894 dt. 11.11.2020) and ICMR Project grant (File No. 17x(3)/Ad-hoc/19/2022-ITR dt. 23.12.2022). Author BD thanks DST, Govt. of India and IASST for the research fellowship. Authors thank Mr Rakesh Ruchel Khanikar, for initial help with the experiments. The authors thank SAIC, IASST for the instrumentation facilities.

References

1 P. J. Butterworth, *Lehninger Principles of Biochemistry*, W. H. Freeman & Co., New York, 2004.
2 P. Li, Y. L. Yin, D. Li, S. W. Kim and G. Wu, *Br. J. Nutr.*, 2007, **98**, 237–252.
3 G. Wu, *Amino Acids*, 2009, **37**, 1–7.
4 S. R. Kimball and L. S. Jefferson, *Am. J. Clin. Nutr.*, 2006, **83**, 500–507.
5 P. Singh P, S. K. Brar, M. Bajaj, N. Narang, V. S. Mithu, O. P. Katare, N. Wangoo and R. K. Sharma, *Mater. Sci. Eng. C*, 2017, **72**, 590–600.
6 D. G. Babar and S. Sarkar, *Appl. Nanosci.*, 2017, **7**, 101–107.
7 C. Ménard-Moyon, V. Venkatesh, K. V. Krishna, F. Bonachera, S. Verma and A. Bianco, *Chem.–Eur. J.*, 2015, **21**, 11681–11686.
8 S. H. Lee, M. K. Gupta, J. B. Bang, H. Bae and H. J. Sung, *Adv. Healthcare Mater.*, 2013, **2**, 908–915.
9 E. Takai, T. Kitamura, J. Kuwabara, S. Ikawa, S. Yoshizawa, K. Shiraki, H. Kawasaki, R. Arakawa and K. Kitano, *J. Phys. D: Appl. Phys.*, 2014, **47**, 285403.
10 S. Yadav, A. K. Sharma and P. Kumar, *Front. Bioeng. Biotechnol.*, 2020, **8**, 127.
11 I. Ramírez-Camacho, O. Flores-Herrera and C. Zazueta, *Mitochondrion*, 2019, **47**, 266–272.
12 Y. Wang, S. Liu, L. Li, H. Li, Y. Yin, S. Rencus-Lazar, S. Guerin, W. Ouyang, D. Thompson, R. Yang, K. Cai, E. Gazit and W. Ji, *J. Am. Chem. Soc.*, 2023, **145**, 15331–15342.
13 N. H. Kim, H. Choi, Z. M. Shahzad, H. Ki, J. Lee, H. Chae and Y. H. Kim, *Nano Convergence*, 2022, **9**, 1–7.
14 R. O. Price, R. Chiavarini, J. F. Kolb and K. H. Schoenbach, *US Pat.*, US8471171B2, 2013.
15 E. Stoffels, A. J. Flikweert, W. W. Stoffels and G. Kroesen, *Plasma Sources Sci. Technol.*, 2002, **11**, 383.
16 R. Kakei, A. Ogino, F. Iwata and M. Nagatsu, *Thin Solid Films*, 2010, **518**, 3457–3460.
17 J. S. Oh, Y. Aranda-Gonzalvo and J. W. Bradley, *J. Phys. D: Appl. Phys.*, 2011, **44**, 365202.
18 G. Fridman, A. Gutsol, A. B. Shekhter, V. N. Vasilets and A. Fridman, Applied plasma medicine, *Plasma Processes Polym.*, 2008, **5**, 503–533.
19 M. Keidar, R. Walk, A. Shashurin, P. Srinivasan, A. Sandler, S. Dasgupta, R. Ravi, R. Guerrero-Preston and B. Trink, *Br. J. Cancer*, 2011, **105**, 1295–1301.
20 N. Y. Babaeva and G. V. Nadis, *Trends Biotechnol.*, 2018, **36**, 603–614.
21 R. R. Khanikar, M. Kalita, P. Kalita, B. Kashyap, S. Das, M. R. Khan, H. Bailung and K. Sankaranarayanan, *RSC Adv.*, 2022, **12**, 9466–9472.
22 H. R. Metelmann, C. Seebauer, V. Miller, A. Fridman, G. Bauer, D. B. Graves, J. M. Pouvesle, R. Rutkowski, M. Schuster, S. Bekeschus and K. Wende, *Clin. Plasma Med.*, 2018, **9**, 6–13.
23 D. Dobrynin, K. Wasko, G. Friedman, A. A. Fridman and G. Fridman, *Plasma Med.*, 2011, **1**, 109–114.

24 K. N. Lee, K. H. Paek, W. T. Ju and Y. H. Lee, *J. Microbiol.*, 2006, **44**, 269–275.
25 H. H. Reitberger, M. Czugala, C. Chow, A. Mohr, A. Burkovski, A. K. Gruenert, R. Schoenebeck and T. A. Fuchsluger, *Am. J. Ophthalmol.*, 2018, **190**, 150–163.
26 Y. A. Keping, J. I. Qikang, C. Zheng, D. E. Guanlei, Y. I. Shengyong and L. I. Zhen, *Plasma Sci. Technol.*, 2018, **20**, 044005.
27 B. H. Adil, M. M. Al-Halbosiy and H. H. Murbat, *The Use of Cold Atmospheric Plasma in Pentostam Enhancement as Leishmaniasis Treatment In Vitro*, AIP Publishing, Maryland, 2019.
28 S. Lata, S. Chakravorty, T. Mitra, P. K. Pradhan, S. Mohanty, P. Patel, E. Jha, P. K. Panda, S. K. Verma and M. Suar, *Mater. Today Bio*, 2022, **13**, 100200.
29 L. Xu, H. Hou, B. Farkas, K. M. Keener, A. L. Garner and B. Tao, *LWT*, 2021, **149**, 111995.
30 R. R. Khanikar, P. Kalita, M. Narzary, D. Basumatary, A. J. Bharati, A. Priyadarshi, R. Swaminathan, H. Bailung and K. Sankaranarayanan, *RSC Adv.*, 2022, **12**, 26211–26219.
31 J. Y. Jeong, S. E. Babayan, V. J. Tu, J. Park, I. Henins, R. F. Hicks and G. S. Selwyn, *Plasma Sources Sci. Technol.*, 1998, **7**, 282.
32 Y. Ito, K. Urabe, N. Takano and K. Tachibana, *Appl. Phys. Express*, 2008, **1**, 067009.
33 E. J. Szili, S. A. Al-Bataineh, P. M. Bryant, R. D. Short, J. W. Bradley and D. A. Steele, *Plasma Processes Polym.*, 2011, **20**(8), 38–50.
34 M. Hasani, M. R. Khani, M. Karimaei, K. Yaghmaeian and B. Shokri, *J. Environ. Health Sci. Eng.*, 2019, **17**, 1185–1194.
35 L. Wu, Q. Xie, Y. Lv, Z. Wu, X. Liang, M. Lu and Y. Nie, *Water*, 2019, **11**, 1818.
36 M. S. Khan, E. J. Lee and Y. J. Kim, *Sci. Rep.*, 2016, **6**, 37072.
37 Reema, R. R. Khanikar, H. Bailung and K. Sankaranarayanan, *Front. Phys.*, 2022, **10**, 942952.
38 J. Li, C. Ma, S. Zhu, F. Yu, B. Dai and D. Yang, *Nanomaterials*, 2019, **9**, 1428.
39 B. Mehravani, A. I. Ribeiro, U. Cvelbar, J. Padrão and A. Zille, *ACS Appl. Polym. Mater.*, 2022, **4**, 3908–3918.
40 S. E. McNeil, *Characterization of Nanoparticles Intended for Drug Delivery*, Humana Press, New York, 2010.
41 A. Sankhla, R. Sharma, R. S. Yadav, D. Kashyap, S. L. Kothari and S. Kachhwaha, *Mater. Chem. Phys.*, 2016, **170**, 44–51.
42 P. L. Gentili, F. Ortica and G. Favaro, *J. Phys. Chem. B*, 2008, **112**, 16793–16801.
43 L. Maggini and D. Bonifazi, *Chem. Soc. Rev.*, 2012, **41**, 211–241.
44 F. Geng, L. Zheng, L. Yua, G. Li and C. Tung, *Process Biochem.*, 2010, **45**, 306–311.
45 A. P. Demchenko, *Luminescence*, 2002, **17**, 19–42.
46 H. R. Shen, J. D. Spikes, P. Kopečeková and J. Kopeček, *J. Photochem. Photobiol., B*, 1996, **34**, 203–210.
47 B. B. Ivanova, *Spectrochim. Acta, Part A*, 2006, **64**, 931–938.
48 C. N. Banwell, *Fundamentals of Molecular Spectroscopy*, McGRAW-Hill, New York, 1966.
49 T. Tanaka, *Bull. Chem. Soc. Jpn.*, 1972, **45**, 2113–2120.
50 D. L. Pavia, G. M. Lampman, G. S. Kriz and J. A. Vyvyan, *Introduction to Spectroscopy*, Cengage Learning, USA, 2014.
51 S. C. Jeyaseelan and A. M. Benial, *J. Mol. Recognit.*, 2021, **34**, 2872.
52 C. R. Carubelli, A. M. Massabni and S. R. Leite, *J. Braz. Chem. Soc.*, 1997, **8**, 597–602.
53 K. Sankaranarayanan, A. Dhathathreyan, J. Krägel and R. Miller, *J. Phys. Chem. B*, 2012, **116**, 895–902.
54 G. Kell and H. Steinhart, *J. Food Sci.*, 1990, **55**, 1120–1123.
55 P. Singh, N. Narang, R. K. Sharma and N. Wangoo, *ACS Appl. Bio Mater.*, 2020, **3**, 6196–6203.